The ball-on-three-balls strength test: In-situ testing through X-ray radiography and tomography

Maximilian Staudacher, Gustavo Pinzón, Jérôme Adrien, J. Lachambre, E Maire, Jérôme Chevalier, Tanja Lube

Open Ceramics 17 (2024) 100514

Contents lists available at ScienceDirect

Open Ceramics

journal homepage: www.sciencedirect.com/journal/open-ceramics

The ball-on-three-balls strength test: In-situ testing through X-ray radiography and tomography

Maximilian Staudacher [a], Gustavo Pinzón [b], Jérôme Adrien [b], Joël Lachambre [b], Eric Maire [b], Jérôme Chevalier [b], Tanja Lube [a,*]

[a] Department of Materials Science, Montanuniversität Leoben, Franz Josef-Strasse 18, Leoben, 8700, Austria
[b] University of Lyon, INSA-Lyon, MATEIS UMR CNRS 5510, 20 Avenue Albert Einstein, Villeurbanne, 69621, France

ARTICLE INFO

Handling Editor: Dr P Colombo

Keywords:
Strength testing
Biaxial testing
Ball-on-Three-Balls-Test
In-situ-testing
X-ray tomography

ABSTRACT

Over the past two decades, the Ball-on-Three-Balls-test (B3B) has been increasingly used due to its low systematic error and simple execution. A limiting factor for a more wide-spread use of the B3B-test is the lack of an accurate analytical solution. This demands the use of numerical methods, such as Finite-Element-Analysis (FEA). In a recent work, FEA has been used to assess the influence of non-linear effects on the measured strength. To validate the utilized FEA-model, the experimental measurement of the specimen's deflection can be drawn on. Due to the design of the fixture for the B3B-test, common deflection-measurement methods are not straightforward. Therefore, X-ray tomography is employed in this paper to track the displacement of the load and support balls for thin plates of a high-strength glass and Ce-doped zirconia presenting transformation-induced plasticity. Furthermore, the ball displacement is also determined from two-dimensional radiographs and shows good agreement with FEA results.

1. Introduction

Biaxial testing is fundamental in assessing the mechanical strength of brittle materials like ceramics and glasses. Several well-known methods include the Ring-on-Ring-test, the Ball-on-Ring-test, the Piston-on-Three-Balls-test, or the Ball-on-Three-Balls-test [1–11]. In recent years, the Ball-on-Three-Balls-test (B3B) has gained popularity due to its low systematic error and simplicity. However, its broader adoption is hindered by the lack of an accurate analytical solution to describe the stress and deflection field. While the analytical solution for other ball-loaded tests, such as the Ball-on-Ring-test, can provide reasonably accurate maximum stress values for the B3B test [12,13], numerical methods like Finite-Element Analysis (FEA) are often necessary to evaluate stresses and deflection precisely.

In a recent study of the B3B-test, the influence of load dependent, non-linear effects on the measured strength was examined [14]. Two major effects were analyzed both qualitatively and quantitatively. Firstly, the contact area between the loading ball and the specimen increases as the load and deflection increase. This causes a deviation from an ideal, punctiform load introduction (that is usually assumed for stress evaluation via FEA) towards a Hertzian surface load distribution. Thus, the leverage and the applied bending moment are altered. Secondly, specimen deflection causes the contact point between the support balls and the specimen to shift towards the specimen center. Again, this changes the leverage and applied bending moment. Both effects collectively reduce the applied bending moment and the maximum tensile stress σ_{max}. Neglecting these effects can result in an overestimation of the material's strength (this aspect is relevant for other testing methods as well, especially if the stress evaluation is based on analytical solutions). Fig. 1 illustrates this effect for high-strength, low Young's modulus glass specimens. Particularly for thin specimens, the combination of these effects can lead to a 20 % decrease in normalized stress, resulting in a 20 % overestimation of the material's strength.

These findings, derived from FEA and theoretical analysis, were implemented through correction factors in the current evaluation of the maximum stress for the B3B-test. Analytical expressions were introduced for both effects, reducing the maximum tensile stress accordingly. These correction factors were validated using non-linear FEA for a wide range of specimen geometries and materials. Excellent agreement for specimens with a relative thickness (i.e. the specimen's thickness divided by the support radius) $\geq$0.1 was demonstrated [14]. However, the correction factors or the non-linear FEA model have not yet been

* Corresponding author.
E-mail address: tanja.lube@unileoben.ac.at (T. Lube).

https://doi.org/10.1016/j.oceram.2023.100514
Received 17 October 2023; Received in revised form 22 November 2023; Accepted 22 November 2023
Available online 25 November 2023

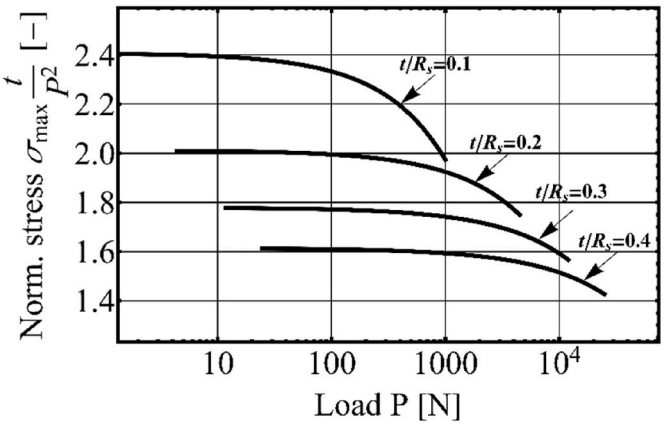

Fig. 1. Reduction in normalized maximum tensile stress in B3B-tests as a function of the applied load P for different relative specimen thicknesses t/R_S. These FEA-results are applicable to a specimen with a radius R of 12 mm, a support radius R_S of 10 mm, Poisson's ratio ν of 0.22 and Young's modulus E of 70 GPa. The thickness t of the specimen ranged from 0.5 mm to 4 mm. Figure adapted from Ref. [14].

validated through experimental results.

Therefore, the objective of this study is to validate the FEA model for non-linear cases. To achieve validation, the experimentally determined specimen deflection was chosen as a suitable benchmark. Common methods, like Digital Image Correlation (DIC) or Linear Variable Differential Transformers (LVDT), cannot be implemented in a straightforward way due to the B3B-test fixture's design [15–18]. Implementing these methods would require adjustments to the fixture and overall testing setup, potentially compromising test advantages and comparability to the regular setup. Hence, an alternative method with minimal impact on the testing setup was sought, using X-ray tomography and radiography.

In this study, X-ray tomography is used to track the three-dimensional displacement of the load and support balls. This method involves incrementally increasing the load, with each tomography recording being taken at a constant load level. In parallel, the positions of the balls in three-dimensional space are determined from two-dimensional radiographs. The latter approach significantly reduces experimental time and allows for in-situ image acquisition without the need to hold at constant load levels. The experiments were conducted on thin, high strength glass plates to highlight the influence of non-linear effects and to observe substantial deflections. Additionally, Ce-doped zirconia, which exhibits some degree of ductility due to Transformation Induced Plasticity (TRIP, see Refs. [19,20]) was investigated to evaluate the effect of the material's non-linearity during the B3B-test.

2. Experimental methods

2.1. Specimen preparation

The glass specimens were sourced from Schott AG (Hattenbergstrasse 10, 55,122 Mainz, Germany) and are commercially available under the product name AF32®eco. The specimens were cut into squares with an edge length of 10 mm. Each specimen has a thickness of 130 μm in its as-delivered state, and neither the thickness nor surface was modified. The material's mechanical properties are given in Ref. [21].

For the zirconia specimens, a composite consisting of ceria-stabilized zirconia, alumina and aluminates was utilized [20,22]. The material is commercially available under the product name EvoCera® from Doceram GmbH (Heβlingsweg 65–69, 44,309 Dortmund, Germany). Specimens were received as discs with a diameter of 20 mm. They were cut to squares with an edge length of 10 mm, ground and polished to a thickness of approximately 280 μm. Special care was taken during the polishing process to prevent phase transformation before testing. The monoclinic phase content of each specimen was assessed through X-ray diffraction (XRD) to ensure a low initial monoclinic content and high transformability. An average monoclinic content of about 6 % was determined.

2.2. Testing setup

To conduct in-situ bending experiments, a tension/compression device as detailed in Ref. [23] was employed. The testing fixture is enclosed within a transparent PMMA tube with an outer diameter of 30 mm and a 2 mm wall thickness. The tube is fastened to a compression/tension stage with a 5 kN load cell. The testing fixture itself is held in place through a compression fit to a steel rod on both the upper and lower stamps, depicted schematically in Fig. 2. Each specimen was loaded until failure, with a discontinuous load increase and holding times of up to 30min for tomography specimens. For radiography specimens, a constant displacement rate of 1 μm/s was used. In both cases, the load was recorded at 1 Hz.

The testing fixture is a modified version of the B3B-fixture described in Refs. [15–18]. It's components and a schematic of the testing setup shown in Fig. 2a) and b). Two major adjustments were made to enable in-situ testing and X-ray observation. First, materials were chosen to minimize absorption and the fixture's impact. The fixture was constructed from POM, as depicted in Fig. 2. For the load- and support balls, high-performance bearing balls made of Si_3N_4 with a 7.14 mm diameter were used, resulting in a support radius of 4.12 mm. Second, the typical multi-step loading process was reduced to a single step, because access to the fixture was not possible once inside the PMMA tube. This change allowed for minor misalignments in the testing setup, which could be monitored through the resulting X-ray scans. To accommodate the high deformation of the glass specimens, Si_3N_4 spacers were used to raise the loading ball's height and enable larger deflection before contact with the fixture. A radiograph of the testing setup before loading is presented in Fig. 3.

2.3. Tomography analysis

X-ray tomography was employed to image the specimen at several stages of the bending test. For each scan, numerous projections were taken at equally spaced angular positions at a constant load. These projections were then processed using a filtered-back projection algorithm to create a three-dimensional volume. The specimens were imaged using the Vtomex tomograph by phoenix|x-ray systems (Niels-Bohr-Strasse 7, Wunstorf 31515, Germany) at Laboratoire MATEIS (INSA Lyon, France) [24–27]. The scanning parameters for each experiment are provided in Table 1.

Volume reconstruction was performed using the Phoenix system's proprietary software, "datos|x", version 2.0. Prior to reconstruction, the offset from the ideal rotational axis was corrected, and a multi-material filter, a beam hardening correction and a low noise filter were applied.

Using the reconstructed volume, the positions of the balls in three-dimensional space were determined for each load step. This process was performed in ImageJ, version 1.53t, utilizing built-in extensions and plug-ins developed at the MATEIS laboratory. Initially, the stack of images was converted from 16-bit grayscale to 8-bit grayscale. Subsequently, a three-dimensional median filter with a 2-pixel radius was applied. A threshold value was set to separate the balls and specimen from the surrounding image, generating a binary image. After binarization, an opening operation (erosion followed by dilation) based on Euclidean distance measurement was performed. The dilation radius chosen was slightly smaller than the erosion radius to ensure that the balls were no longer in contact with each other and could be individually labeled. Finally, the volume and center of mass were calculated for each labeled ball.

Subsequent data analysis was performed using Mathematica 13.1

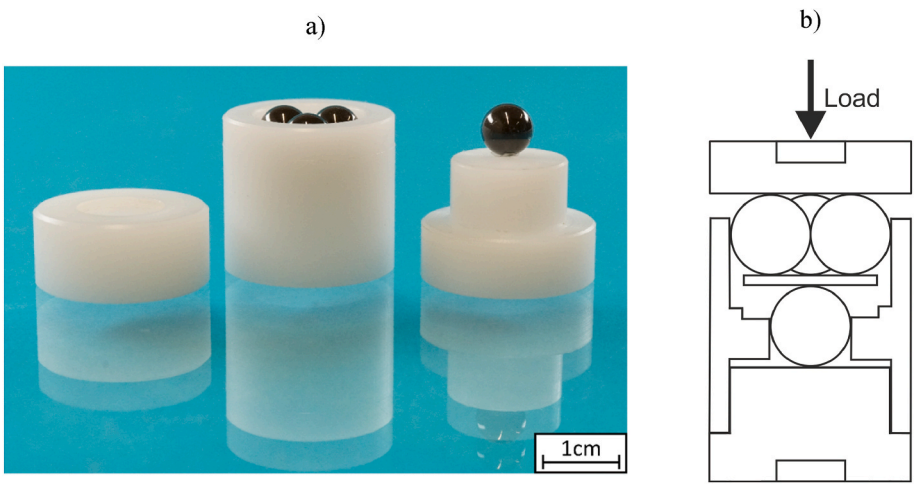

Fig. 2. The testing fixture's components are depicted in a), including the top stamp, guide, bottom stamp (from left to right), and Si3N4 balls for load application. A schematic of the assembly of these components with a loaded specimen is presented in b).

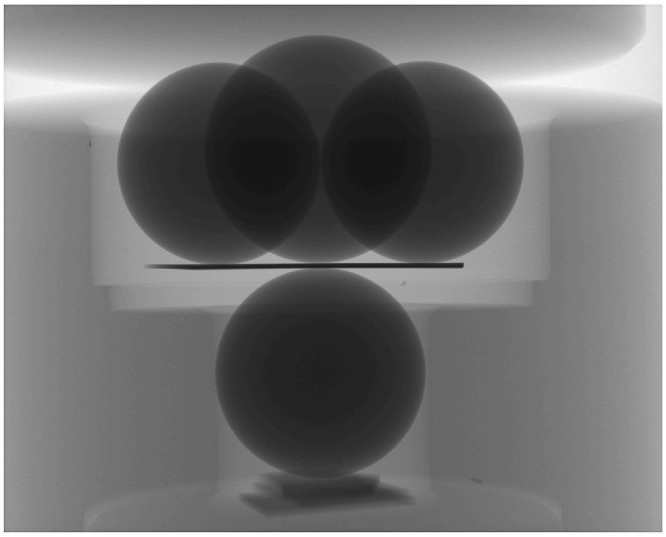

Fig. 3. Radiograph of the testing setup with an undeformed glass specimen and Si_3N_4 spacers beneath the loading ball (ball diameter = 7.144 mm).

Table 1
Equipment parameters for X-ray analysis: Three radiographs were averaged for each of the 900 angular positions, with one radiograph skipped.

Parameter	Glass	Zirconia
Number of projections	900	900
Voltage	80 kV	140 kV
Current	280 μA	80 μA
Voxel size	11.91 μm	11.91 μm
Exposure time	333 ms	500 ms
Tomography scanning time	20min	30min

from Wolfram Research, Inc. (100 Trade Center Drive, Champaign IL 61820-7237, USA). For each tomograph, the vertical distance between the support balls and the loading ball was determined and their positions examined for any deviations from the ideal setup. In the results presented in this study, no significant misalignments were detected. If the testing fixture was tilted, the measured distances were corrected accordingly.

2.4. Radiograph analysis

While X-ray tomography is ideal to measure the 3D position of the balls during the test, the loading system must pause at each scanning point. This may affect the specimen's mechanical response (e.g., through sub-critical-crack-growth) and significantly increase the time needed for a complete experimental campaign. Recent techniques propose using radiographs instead of 3D reconstructed volumes to measure the process's kinematics [28], substantially reducing the time required. Following a similar approach, this study uses the open-source technique proposed by Andò et al. [29], where the 3D position of a sphere is measured using a single radiograph for conic-beam tomographs. In summary, the technique involves creating a virtual sphere at a specific distance from the X-ray source, projecting it onto the X-ray detector. By performing a convolution between the measured and virtual radiographs, an estimate of the 3D position of the spheres is obtained. In this study, the distance of the virtual sphere relative to the source was varied in steps of 200 μm, and the reported 3D positions correspond to the scenarios where the convolution peaks exhibited higher values. Further details are available in Ref. [30], and the open-source code is accessible in Ref. [31].

Fig. 4a) displays the radiograph from Fig. 3 after applying the calibration which allows to transform attenuation values to X-ray path length through the balls. This calibration is performed by imaging an individual sphere outside of the experimental setup and fitting an attenuation law to the log-normalized radiograph. The proposed measuring method retrieves the 3D coordinates of the balls. To assess measurement quality, the balls are back-projected onto the detector, generating a virtual radiograph (Fig. 4b) for comparison to the measured radiograph in Fig. 4a. Differences between the two images are quantified by measuring the residual (squared difference) as shown in Fig. 4c). Since the technique does not consider the presence of the specimen, it is absent from the virtual radiograph in Fig. 4b. Notably, this technique was used only on the glass specimens due to the zirconia specimen's higher attenuation coefficient than that of the bearing balls. This caused a substantial error in convolutions between measured and virtual radiographs.

To further assess the quality of 3D measurements using this technique, ball positions were computed from the initial tomography scan at constant load, prior to any loading. During the tomography scan, the setup was rotated along the vertical axis, and at each angular position, a different radiograph was taken. Fig. 5 illustrates the temporal evolution of the position for each ball of the testing assembly along the horizontal plane. As expected, the three support balls exhibit a circular path, while the loading ball shows minimal movement. All radiographs were

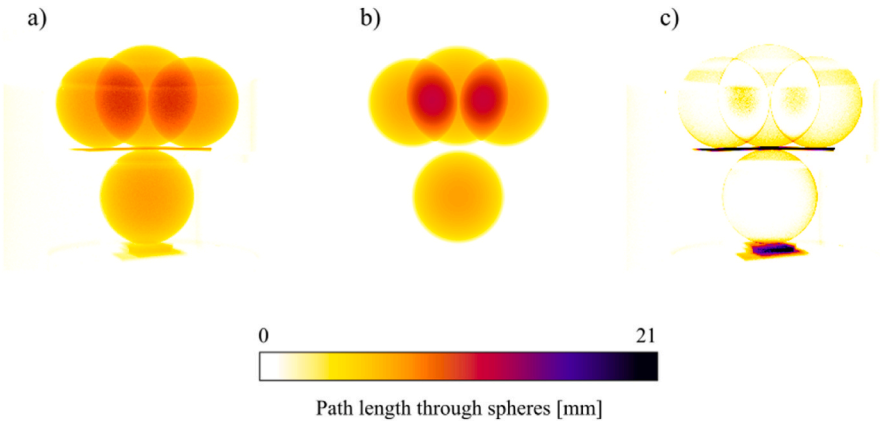

Fig. 4. Measurement of three-dimensional ball positions using radiographs. a) shows the original radiograph after calibration, b) presents a synthetic radiograph generated with the measured ball positions, and c) displays the residual of correlations between the two images. The scale refers to a) and b), with the same color-code applied for the residual's value (in mm^2) in c). (For interpretation of the references to color in this figure legend, the reader is referred to the Web version of this article.)

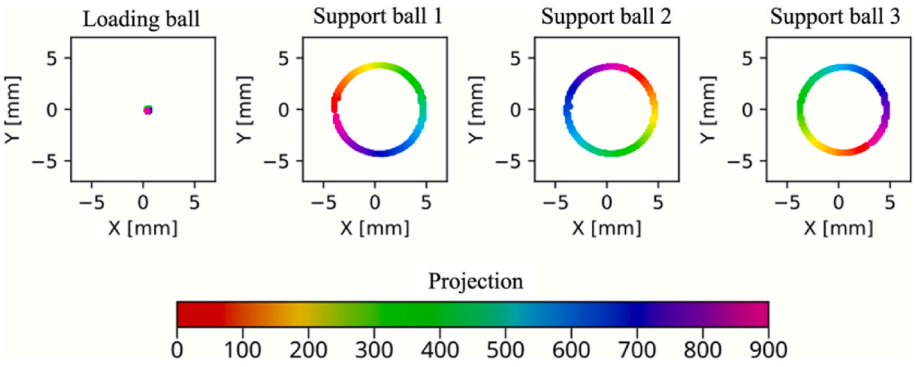

Fig. 5. Temporal evolution of ball positions in the horizontal (XY) plane during a tomography scan: The leftmost graph gives the loading ball's position, while the other graphs depict the position of each support ball.

obtained using the same equipment and machine parameters as given in Table 1. During the compression test, three images were acquired per second, resulting in over 2000 radiographs for each tested specimen.

3. Numerical methods

The primary FEA-model used in this study is shown in Fig. 6a). Due to the problem's symmetry, modeling only half of the setup is sufficient. The model was implemented in ANSYS Mechanical Release 2022R1 by ANSYS Inc. (Southpointe 2600 Ansys Drive, PA 15317, Canonsburg, USA) using an APDL (Ansys Parametric Design Language) script. This approach provides detailed control of the model and complete documentation of all input parameters and model changes. The model consisted of approximately 50,000 SOLID186 20-node brick elements and 200,000 nodes (the exact numbers depend on the specimen's thickness). The contact between the balls and the specimen was modeled through symmetrical contact using CONTA174 and TARGE170 elements, with a friction coefficient of 0.5. A mesh convergence analysis was conducted for specimen deflection to ensure consistent results.

The model considers the interaction between the balls and the

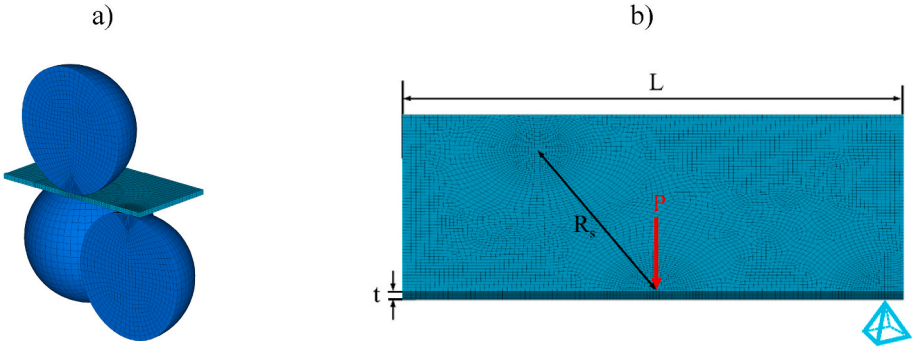

Fig. 6. a) depicts the meshed FEA model used for non-linear analysis, which includes the loading balls, support balls and the glass specimen, serving as a base of comparison to the experimental results. b) shows the linear model with L as the edge length of the specimen, t as its thickness and R_S as the support radius determined by the support ball radii [14].

specimen, allowing for the inclusion of non-linear effects. The term "non-linear effects" encompasses the change in contact area between the balls and the specimen and the influence of friction in these regions. Furthermore, the geometrically non-linear deformation of the specimen and consequent shift of the contact points to the support balls is included as well.

Additionally, a model used in previous work (Model 2 in Ref. [14] for further details on the mesh and convergence analysis) was employed to analyze the linear behavior of the specimen, as shown in Fig. 6b). This model serves as a reference for an idealized testing situation involving punctiform load application and boundary conditions. Importantly, this model does not consider the non-linear geometrical behavior, and its results are independent of the magnitude of the applied load. Both models assume linear-elastic material behavior.

4. Results

4.1. Tomography

Fig. 7 compares tomography and numerical results for glass specimens. More specifically, the vertical distance between the loading balls' center and the support balls' center is given as a function of the applied load. In the experimental results, the distance at 0 N is defined through the balls' diameter and the specimen's thickness, as a load-free setup could not be scanned (the fixture moves during tomography scans, thus unsettling the testing setup if not loaded at all).

Fig. 8a) shows the comparison between the experimental and numerical results for the Ce-doped zirconia specimen. Note the good agreement of experiments with both models up to 28 N and the substantial deviation from both at that load. Fig. 8b) displays the corresponding tensile-loaded surface after failure, examined with an BX53 M optical light microscope by Olympus K.K. (2-3-1 Nishi-Shinjuku, 163–0914 Tokyo, Japan). Utilizing differential interference contrast, regions of phase transformation are made visible due to an increase in volume and the formation of surface structures. Phase transformation is observed within a circular region at the specimen's center (approximately 5 mm in diameter) and near the crack path up to the specimen's edge. This is in line with previous findings in literature [19,20].

4.2. Radiography

Fig. 9a) and Fig. 9c) present results from radiograph analysis in comparison to linear and non-linear FEA. Note that for better visualization, only every twentieth measurement from the experimental data is shown. The maximum load has doubled compared to tomography

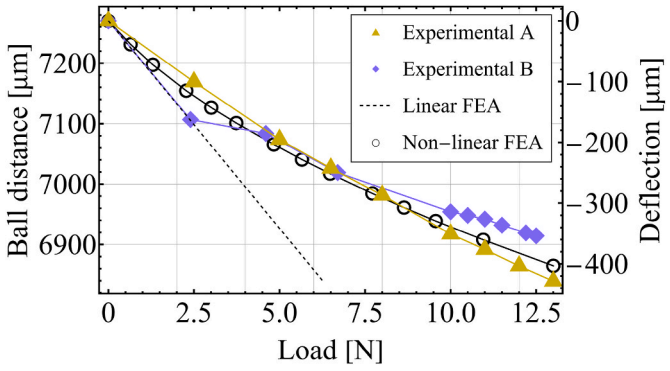

Fig. 7. Comparison of the vertical distance between the loading ball center and the support ball center from experimental results, linear FEA and non-linear FEA. The experimental results were obtained for two glass specimens using tomography, with glass specimen A in yellow and glass specimen B in purple. (For interpretation of the references to color in this figure legend, the reader is referred to the Web version of this article.)

experiments. While tendencies align closely with non-linear FEA, there is an offset of approximately 190 µm in the ball distance at 1 N for both specimens. The origin of such an offset is discussed in the following section. Correcting each measured distance by this difference, Fig. 9b) and d) are obtained. This correction eases a comparison of the tendencies between the experimental measurements and non-linear FEA results. With increasing load, higher deflections are measured compared to FEA. A maximum deflection of about 620 µm and 580 µm was measured for specimen C and D, respectively, exceeding 4 times the specimen's thickness. The resulting deformation is shown in Fig. 10c), along with the deformation in the initial state and at half of the failure load in Fig. 10a) and b), respectively.

5. Discussion

For glass specimens, the experimental results from tomography show excellent agreement with the non-linear FEA model, which includes the effects of friction, the change in contact area and contact location due to load. Initially, alignment with the linear model is observed, but deviations occur beyond 3 N. As the load increases, the specimen's deflection decreases relative to the linear model's prediction, consistent with the non-linear model and prior work [14]. Experimental results from both tests deviate by a maximum of 20 µm from non-linear FEA. Note that the experimentally determined parameter was the full distance between the loading and support balls, around 7200 µm. In this context, a 20 µm difference to FEA is less than 0.3 % of the total measured distance. However, when focusing solely on deflection (ranging from 300 µm to 400 µm), the 20 µm difference corresponds to an error of about ±6 %.

For the zirconia specimen, a direct comparison to FEA is challenging, given that the utilized model lacks implementation of phase transformation. More precisely, a significant non-linear *increase* of the deflection with increasing load was observed, indicating the onset of the TRIP-effect at approximately 28 N. This aligns with theoretical considerations, where plastic deformation through phase transformation leads to increased deformation without the expected increase in load. As displayed in Fig. 8b), phase transformation is evident in highly stressed regions. Due to the higher stiffness of the zirconia specimen, the total deflection (about 100 µm) is much smaller than for glass specimens, resulting in a larger relative error.

The overall results from the radiograph analysis closely align with those from tomography and simulations, but with a 190 µm offset for the vertical distance between radiographs measurements and simulation. The experimental error for measuring the 3D position is ±40 µm for each ball due to the 200 µm discretization of virtual sphere positions for convolution. However, this doesn't fully account for the entire offset. Another source of error is the image calibration procedure, performed outside the B3B-test setup using a single sphere. The presence of the stamps and the fixture alters measured attenuation values on radiographs, affecting calibration quality and 3D measurement. This difference is notable compared to previous applications where testing setups were made of low-attenuation materials, not interfering with calibration [30]. The primary advantage of measuring the 3D position of balls directly from radiographs is a significant reduction in experimental and analysis time. While full 3D volume measurement takes almost half a day for several scans, this alternative provides >2000 scans within a few minutes. This accelerated experimental procedure allows for higher maximum loads and increased deformation, as effects like sub-critical crack growth become less significant [32,33].

Currently, the accuracy of this method (or these two approaches) falls short of offering a viable alternative to well-established methods for measuring deflection, especially when dealing with specimen deformations in the range of a few micrometers. However, for specific use cases like the B3B-test, where established methods are impractical, and specimens with substantial deformations, it presents a promising alternative.

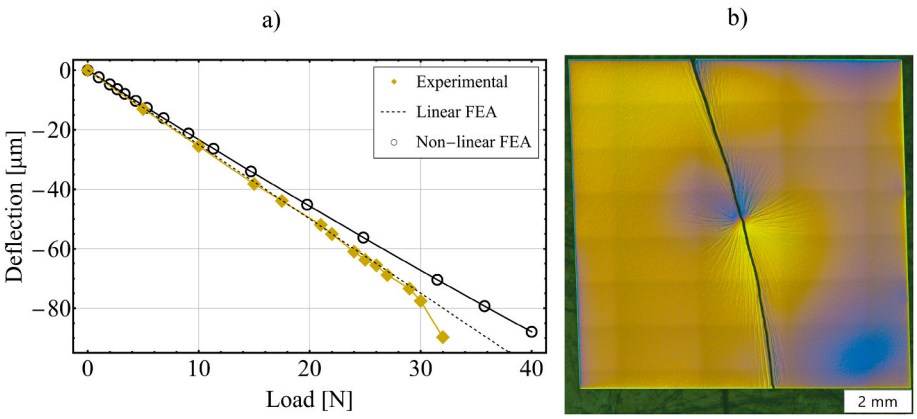

Fig. 8. a) compares the vertical distance between the loading ball center and the support ball center for a Ce-doped zirconia specimen to experimental results obtained through tomography. b) displays the fractured specimen, with transformed regions visible as surface undulations.

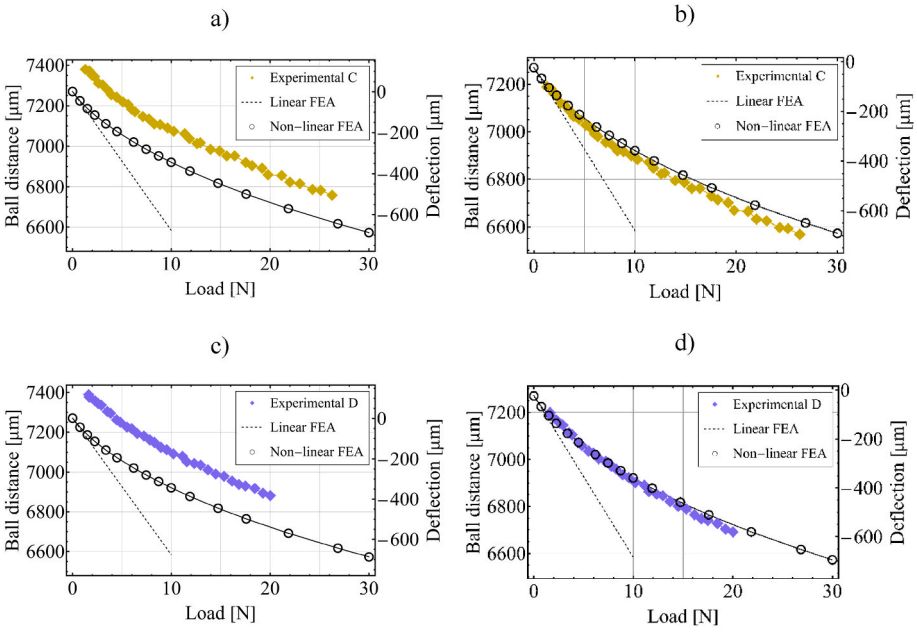

Fig. 9. Comparison of the vertical distance between the loading ball center and the support ball canter for experimental results, linear FEA and non-linear FEA. The experimental results for glass specimens C and D were obtained through radiography. Uncorrected values for specimen C are given in a), and values corrected by a 190 µm offset are given in b). For specimen D, uncorrected values are given in c), and corrected values are given in d).

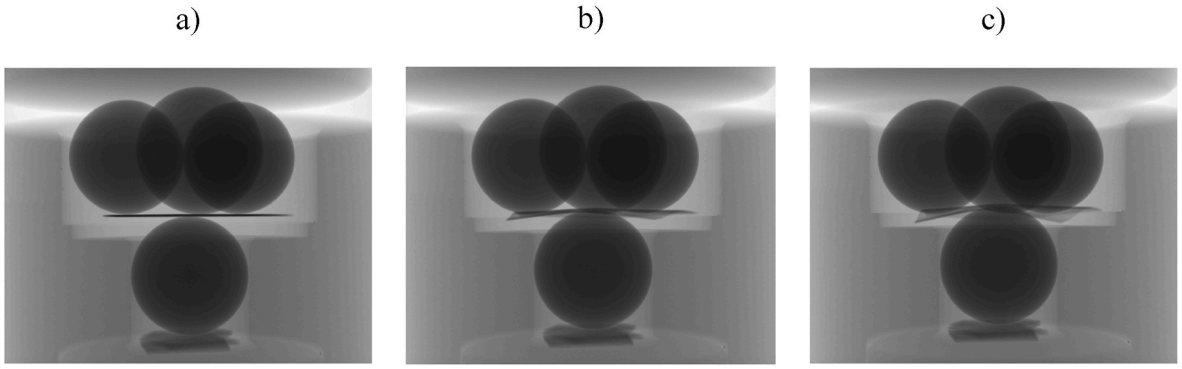

Fig. 10. Radiographs of glass specimen C at 1 N (a)), 13 N (b)) and 26.6 N (c)), highlighting the substantial deflection of the specimen, especially in c) (ball diameter = 7.144 mm).

This method's first iteration could be enhanced by using a more suitable load cell. For the investigated specimens, which fractured at less than 50 N, the range of the load cell was not ideal. Another improvement is increasing the sampling rate for load measurement, which is currently limited to 1 Hz.

In summary, FEA predictions align well with experimental data, particularly for glass specimens. Thus, the results from this study provide valuable experimental validation for comparisons and conclusions drawn in earlier work, notably in Ref. [14]. Nonetheless, challenges remain to accurately model the non-linear behavior caused by phase transformation.

6. Summary

This work serves as a follow-up to a previous publication on the Ball-on-Three-Balls-test [14]. That publication discussed and quantified the influence of non-linear effects on the measured strength through Finite-Element-Analysis (FEA). To validate these theoretical findings experimentally, deflection measurements via X-ray tomography were employed in the present work.

The specimen's deflection is determined from a three-dimensional reconstruction (tomograph) of the specimen and load/support balls. Two-dimensional radiographs provide a continuous alternative to discontinuous tomography measurements. Through this approach, the amount of deflection data is substantially increased.

In general, excellent agreement between the deflection obtained through tomography and through FEA was observed. While radiography measurements align well with general tendencies, the absolute values differ from FEA, showing a systematic offset of about 190 μm.

In general, measuring the deflection of thin, flexible ceramic specimens through X-ray tomography or radiography holds promise. However certain aspects require improvement before these methods are a suitable alternative to well-established methods. Nonetheless, the validity of FEA was demonstrated, thereby validating findings from previous work.

Data availability

Data will be made available on request.

Declaration of competing interest

The authors declare that they have no known competing financial interests or personal relationships that could have appeared to influence the work reported in this paper.

Acknowledgements

M. Staudacher gratefully acknowledges financial support by the Austrian BMVIT and BMWFW in the project "CharAM" (FFG 877684) of the COIN/IraSME program. The authors are grateful to the JECS Trust for funding the visit of M. Staudacher to INSA Lyon (Contract No. 2022305). The authors further thank SKF Austria AG for providing the Si_3N_4 bearing balls.

References

[1] ASTM C 1499-05, Test Method for Monotonic Equibiaxial Flexural Strength of Advanced Ceramics at Ambient Temperature, ASTM International, West Conshohocken, PA, 2005.
[2] R. Morrell, Biaxial Flexural Strength Testing of Ceramic Materials: A National Measurement Good Practice Guide No. 12, National Physical Laboratory, 2007.
[3] G. With, H.H.M. Wagemans, Ball-on-ring test revisited, J. Am. Ceram. Soc. 72 (1989) 1538–1541.
[4] H.L. Frandsen, The small displacement elastic solution to the ball-on-ring testing method, Mech. Mater. 55 (2012) 33–40.
[5] C.W. Huang, C.H. Hsueh, Piston-on-three-ball versus piston-on-ring in evaluating the biaxial strength of dental ceramics, Dental materials official publication of the Academy of Dental Materials 27 (2011) e117–e123.
[6] Y. Torres, R. Bermejo, F.J. Gotor, E. Chicardi, L. Llanes, Analysis on the mechanical strength of WC-Co cemented carbides under uniaxial and biaxial bending, Mater. Des. 55 (2014) 851–856.
[7] M. Staudacher, T. Lube, J. Schlacher, P. Supancic, Comparison of biaxial strength measured with the Ball-on-Three-Balls- and the Ring-on-Ring-test, Open Ceramics 6 (2021), 100101.
[8] J. Malzbender, R.W. Steinbrech, Fracture test of thin sheet electrolytes for solid oxide fuel cells, J. Eur. Ceram. Soc. 27 (2007) 2597–2603.
[9] W. Adler, D. Mihora, Biaxial flexure testing: analysis and experimental results, in: Fracture Mechanics of Ceramics, pp. 227–245..
[10] R. Morrell, N.J. McCormick, J. Bevan, M. Lodeiro, J. Margetson, Biaxial disc flexure – modulus and strength testing, Br. Ceram. Trans. 98 (2013) 234–240.
[11] J.d.S. Ramos, S. Fraga, G.F. Vogel, L.G. May, Influence of the geometry of ceramic specimens on biaxial flexural strength: experimental testing and finite element analysis, Cerâmica 64 (2018) 120–125.
[12] A.F. Kirstein, R.M. Woolley, Symmetrical bending of thin circular elastic plates on equally spaced point supports, J. Res. Natl. Bur. Stand. Sect. C Eng. Instrum. 71C (1967).
[13] M. Staudacher, P. Supancic, T. Lube, The Ball-on-Ring-test: enhancing an analytical solution by numerical analysis for elastic deformation and small displacements, J. Eur. Ceram. Soc. 43 (2023) 7167–7177.
[14] M. Staudacher, T. Lube, P. Supancic, The Ball-on-Three-Balls strength test for discs and plates: extending and simplifying stress evaluation, J. Eur. Ceram. Soc. 43 (2023) 648–660.
[15] W. Harrer, R. Danzer, P. Supancic, T. Lube, The ball on three balls test: strength testing of specimens of different sizes and geometries, Proceedings 10th ECerS Conf (2008) 1271–1275.
[16] R. Danzer, P. Supancic, W. Harrer, Der 4-Kugelversuch zur Ermittlung der biaxialen Biegefestigkeit spröder Werkstoffe, Kriegsmann, J. (Hrsg): Technische keramische Werkstoffe (2009) 1–48.
[17] R. Danzer, W. Harrer, P. Supancic, T. Lube, Z. Wang, A. Börger, The ball on three balls test—strength and failure analysis of different materials, J. Eur. Ceram. Soc. 27 (2007) 1481–1485.
[18] A. Börger, P. Supancic, R. Danzer, The ball on three balls test for strength testing of brittle discs: stress distribution in the disc, J. Eur. Ceram. Soc. 22 (2002) 1425–1436.
[19] J. Chevalier, A. Liens, H. Reveron, F. Zhang, P. Reynaud, T. Douillard, L. Preiss, V. Sergo, V. Lughi, M. Swain, N. Courtois, Forty years after the promise of «ceramic steel?»: zirconia-based composites with a metal-like mechanical behavior, J. Am. Ceram. Soc. 103 (2020) 1482–1513.
[20] H. Reveron, M. Fornabaio, P. Palmero, T. Fürderer, E. Adolfsson, V. Lughi, A. Bonifacio, V. Sergo, L. Montanaro, J. Chevalier, Towards long lasting zirconia-based composites for dental implants: transformation induced plasticity and its consequence on ceramic reliability, Acta Biomater. 48 (2017) 423–432.
[21] A.G. Schott, Datasheet AF32®eco. https://www.schott.com/de-at/products/af-32-eco-p1000308/downloads. (Accessed 4 October 2023).
[22] P. Palmero, M. Fornabaio, L. Montanaro, H. Reveron, C. Esnouf, J. Chevalier, Towards long lasting zirconia-based composites for dental implants. Part I: innovative synthesis, microstructural characterization and in vitro stability, Biomaterials 50 (2015) 38–46.
[23] A. Sibellas, J. Adrien, D. Durville, E. Maire, Experimental study of the fiber orientations in single and multi-ply continuous filament yarns, J. Text. Inst. 111 (2020) 646–659.
[24] J. Seuba, E. Maire, J. Adrien, S. Meille, S. Deville, Mechanical properties of unidirectional, porous polymer/ceramic composites for biomedical applications, Open Ceramics 8 (2021), 100195.
[25] E. Maire, P.J. Withers, Quantitative X-ray tomography, Int. Mater. Rev. 59 (2014) 1–43.
[26] T. Lacondemine, J. Réthoré, É. Maire, F. Célarié, P. Houizot, C. Roux-Langlois, C. M. Schlepütz, T. Rouxel, Direct observation of the displacement field and microcracking in a glass by means of X-ray tomography during in situ Vickers indentation experiment, Acta Mater. 179 (2019) 424–433.
[27] A. Bouterf, E. Maire, S. Roux, F. Hild, X. Brajer, E. Gouillart, E. Boller, Analysis of compaction in brittle foam with multiscale indentation tests, Mech. Mater. 118 (2018) 22–30.
[28] H. Leclerc, S. Roux, F. Hild, Projection Savings in CT-based Digital Volume Correlation, Experimental Mechanics, 2015.
[29] E. Andò, B. Marks, S. Roux, Single-projection reconstruction technique for positioning monodisperse spheres in 3D with a divergent x-ray beam, Meas. Sci. Technol. 32 (2021), 95405.
[30] O. Stamati, B. Mark, E. Ando, S. Roux, N. Machicoane, X-Ray Radiography 4D Particle Tracking of Heavy Spheres Suspended in a Turbulent Jet, Zenodo, 2022.
[31] Y. Haouchat, et al., Code repository. https://gricad-gitlab.univ-grenoble-alpes.fr/ttk/radioSphere. (Accessed 4 October 2023).
[32] J.B. Wachtman, M.J. Matthewson, W.R. Cannon, Mechanical Properties of Ceramics, Wiley, Hoboken, New JerseyJ, 2009.
[33] D. Munz, T. Fett, Ceramics: Mechanical Properties, Failure Behaviour, Materials Selection, Springer, Berlin, Heidelberg, 1999.